

# Impact of ice sheet meltwater fluxes on the climate evolution at the onset of the Last Interglacial

H. Goelzer<sup>1\*</sup>, P. Huybrechts<sup>1</sup>, Marie-France Loutre<sup>2</sup>, Thierry Fichefet<sup>2</sup>

<sup>1</sup>Earth System Sciences & Departement Geografie, Vrije Universiteit Brussel, Brussels, Belgium

<sup>2</sup>Université catholique de Louvain, Earth and Life Institute, Georges Lemaître Centre for Earth and Climate Research (TECLIM), Louvain-la-Neuve, Belgium

\*now at: Institute for Marine and Atmospheric research Utrecht, Utrecht University, the Netherlands

Correspondence to: H. Goelzer (heiko.goelzer@vub.ac.be)

## Abstract

Large climate perturbations occurred during the transition between the penultimate glacial period and the Last Interglacial (Termination II), when the ice sheets retreated from their glacial configuration. Here we investigate the impact of ice sheet changes and associated freshwater fluxes on the climate evolution at the onset of the Last Interglacial. The period from 135 to 120 kyr BP is simulated with the Earth system model of intermediate complexity LOVECLIM v.1.3 with prescribed evolution of the Antarctic ice sheet, the Greenland ice sheet and the other Northern Hemisphere ice sheets. Variations in meltwater fluxes from the Northern Hemisphere ice sheets lead to North Atlantic temperature changes and modifications of the strength of the Atlantic meridional overturning circulation. By means of the interhemispheric see-saw effect, variations in the Atlantic meridional overturning circulation also give rise to temperature changes in the Southern Hemisphere, which are additionally modulated by the direct impact of Antarctic meltwater fluxes into the Southern Ocean. Freshwater fluxes from the melting Antarctic ice sheet lead to a millennial time scale oceanic

28 cold event in the Southern Ocean with expanded sea ice as evidenced in some ocean sediment  
29 cores, which may be used to constrain the timing of ice sheet retreat.

30

## 31 **1 Introduction**

32 Understanding the climate and ice sheet evolution during past warm periods in the history of  
33 the Earth may provide important insights for projections of future climate and sea-level  
34 changes. The growing amount of paleo-reconstructions for the Last Interglacial period (e.g.  
35 Govin et al., 2012; Capron et al., 2014) in combination with improved model simulations of  
36 this most recent warm period (e.g. Bakker et al., 2013; Lunt et al., 2013, Langebroek and  
37 Nisancioglu, 2014; Loutre et al., 2014) make it an interesting target for studying the coupled  
38 climate-ice sheet system.

39 According to reconstructions, the Last Interglacial (LIG, from ~130-115 kyr BP) was  
40 characterised by a global annual mean surface temperature of up to 2° C above the pre-  
41 industrial (e.g. Turney and Jones, 2010; Capron et al., 2014) and a sea-level high stand of 6-9  
42 m above the present day (Kopp et al., 2009; Dutton and Lambeck, 2012). As the penultimate  
43 glacial maximum was at least as severe as the Last Glacial Maximum (LGM) in both  
44 hemispheres (EPICA community members, 2004; Svendsen et al., 2004), this implies a large  
45 amplitude glacial-interglacial transition in terms of temperature and ice sheet configuration.  
46 At the onset of the LIG, a rapid warming of ~10°C from the preceding cold state is recorded  
47 in deep Antarctic ice cores (Masson-Delmotte et al., 2011) to have occurred between ~135  
48 kyr BP and 130 kyr BP. Current ice core records from the Greenland ice sheet (GrIS) do not  
49 extend long enough back in time to cover the entire penultimate deglaciation and associated  
50 warming (NEEM community members, 2013), but a similar timing and magnitude of  
51 warming compared to the Antarctic can be reconstructed for sea surface temperatures off the  
52 West European margin (Sánchez Goñi et al., 2012). The warming is closely related with an  
53 ice sheet retreat in both hemispheres. Despite large uncertainties in reconstructions, the global  
54 sea-level stand at 135 kyr BP of as low as -80 m (Grant et al., 2012) is indicative of the large  
55 amount of freshwater that entered the ocean in the form of meltwater from the retreating ice  
56 sheets during Termination II. Aside from determining the amplitude of sea-level changes,  
57 which is the focus of many studies (e.g. Robinson et al., 2011; Stone et al., 2013), the  
58 associated climate impacts and possible feedbacks on the ice sheet evolution of this

59 freshwater forcing are an important element for a process understanding of the coupled  
60 climate-ice sheet changes at that time.

61 A climatic mechanism that is thought to be directly related to changes in the NH ice sheet  
62 freshwater fluxes (FWF) is the interhemispheric see-saw effect (Stocker, 1998) that links SH  
63 warming to a weakening of the Atlantic meridional overturning circulation (AMOC). If the  
64 see-saw effect was active during the onset of the LIG, NH ice sheet melting during  
65 Termination II would have been the cause for a substantial AMOC weakening and NH  
66 cooling, while reduced interhemispheric heat transport would have caused a gradual SH  
67 warming (Stocker and Johnson 2003). The see-saw mechanism was evoked to explain part of  
68 the peak Antarctic warming during the LIG (e.g. Holden et al., 2010; Marino et al., 2015),  
69 even though some Southern Ocean (SO) warming was shown by Langebroek and Nisancioglu  
70 (2014) to be possible with orbital forcing alone (without NH freshwater forcing). The see-saw  
71 mechanism has been speculated to have caused increased Antarctic ice shelf melting and  
72 West Antarctic ice sheet (WAIS) retreat (Duplessy et al., 2007). The retreat of the WAIS,  
73 which is believed to have been grounded at the edge of the continental shelf during the  
74 penultimate glaciation, generated a large anomalous flux of freshwater into the SO. Such  
75 freshwater forcing could have had a substantial influence on the SO configuration in terms of  
76 sea ice extent and ocean circulation as shown in model experiments for the last deglaciation  
77 (Menviel et al., 2011), for future global warming scenarios (Swingedouw et al., 2008) and for  
78 the present day (Bintanja et al., 2013). The impact of increased Antarctic FWF is thought to  
79 consist of a surface ocean freshening, stratification of the surface ocean and cooling, in turn  
80 promoting sea ice growth (e.g. Bintanja et al., 2013) and reduced Antarctic Bottom Water  
81 (AABW) formation (Menviel et al., 2011). Recently, Golledge et al. (2014) suggested that  
82 such a mechanism might also have provided a feedback on Antarctic ice sheet (AIS) retreat  
83 for meltwater pulse 1A during the last glacial-interglacial transition (Termination I), by  
84 promoting warming of mid-depth ocean waters that provide additional heat for melting ice  
85 shelves.

86 In the present work, we study the effect of evolving ice sheet boundary conditions on the  
87 climate, by simulating the climate evolution at the onset and over the course of the LIG with  
88 an Earth system model of intermediate complexity (EMIC). The model is forced with realistic  
89 ice sheet boundary conditions from offline simulations of ice dynamic models of the AIS and  
90 GrIS and reconstructions of the other NH ice sheets. With this study we extend the work of

91 Loutre et al. (2014) by additionally including dynamic ice sheet changes of the GrIS and AIS  
92 and focusing on the effect of ice sheet freshwater fluxes on the climate, particularly in the  
93 Southern Hemisphere (SH). The model and experimental setup are described in section 2 and  
94 3, respectively, followed by results (Sect. 4, 5 and 6), their discussion in section 7 and  
95 conclusions (Sect. 8).

96

## 97 **2 Model description**

98 We use the EMIC LOVECLIM version 1.3, which includes components representing the  
99 atmosphere, the ocean and sea ice, the terrestrial biosphere and the ice sheets (cf. Figure 1).  
100 The model has been utilised in a large number of coupled climate-ice sheet studies (e.g.  
101 Driesschaert et al., 2007; Swingedouw et al., 2008; Goelzer et al., 2011; 2012a; Loutre et al.,  
102 2014) and is described in detail in Goosse et al. (2010).

103 In this study, the climate components are forced by time-evolving ice sheet boundary  
104 conditions, which are calculated off-line, i.e. uncoupled from the climate evolution. Our  
105 modelling approach for the ice sheets consists of a combination of reconstructed NH ice  
106 sheets (except the GrIS) based on geomorphological data (Sec. 2.1) and of standalone ice  
107 dynamic simulations of the GrIS and AIS (Sec. 2.2). In either case, the boundary conditions  
108 provide time evolving topography, ice sheet extent (albedo) and spatially and temporally  
109 variable FWF to the climate model. As common practice for simulations with large amounts  
110 of freshwater input, we conserve global salinity and global volume in the ocean model to  
111 avoid numerical problems.

### 112 **2.1 Northern Hemisphere ice sheet forcing**

113 We have little geomorphological evidence for Northern Hemisphere (NH) ice sheet evolution  
114 during Termination II since it was mostly destroyed by the re-advance leading to the LGM.  
115 Therefore, the reconstruction of NH ice sheet evolution for the period of interest is made  
116 based on information from the last deglaciation. The method was already described in some  
117 detail in Loutre et al. (2014). Nevertheless, we include a more thorough description here  
118 (Appendix A). The resulting boundary conditions used to force the climate model consist of a  
119 chronology of ice mask and surface elevation changes (Figure 2) and freshwater fluxes  
120 (Figure 3b) over the entire LIG period. Support for the derived chronology of NH ice sheet  
121 evolution and their FWF can be found in records of ice-rafted detritus (IRD) from the

122 subpolar North Atlantic (Kandiano et al., 2004; Oppo et al., 2006). These show variability of  
123 similar signature during the deglaciation and in particular a last IRD peak at ~128 kyr BP  
124 preceding low IRD levels throughout the LIG.

## 125 **2.2 Simulations of the Greenland and Antarctic ice sheets**

126 For the present study, the climate components are partially forced by results from stand-alone  
127 simulations of the GrIS and AIS, which have been adapted from existing ice sheet model  
128 experiments (Huybrechts 2002). The configuration of both ice sheet models and the forcing  
129 interface follows the description in Goosse et al. (2010) with the following exceptions.  
130 Forcing for the ice sheet models is derived from scaling present-day observations of  
131 temperature and precipitation with indices based on ice core records, as often done for long-  
132 term paleo ice sheet modelling (e.g. Huybrechts, 1990; Letréguilly et al., 1991; Zweck and  
133 Huybrechts, 2005; Greve et al., 2011). For the GrIS the forcing record was created following  
134 Fürst et al. (2015). We combine a synthesised Greenland  $\delta^{18}\text{O}$  record derived from Antarctica  
135 Dome C using a bipolar seesaw model (Barker et al., 2011) with the NEEM temperature  
136 reconstruction (NEEM community members, 2013) between 128.44 kyr BP and 120 kyr BP.  
137 The Barker  $\delta^{18}\text{O}$  record is converted to a spatially uniform temperature anomaly with a  
138 constant temperature/ isotope factor  $\Delta T = 2.4 \text{ }^\circ\text{C}/\text{‰} * (\delta^{18}\text{O} + 34.83)$  as in Huybrechts (2002).  
139 Positive temperature anomalies of the NEEM record are scaled by a factor 0.6 to fulfil  
140 constraints on maximal ice sheet retreat from Camp Century and Dye3 ice core locations that  
141 are assumed to have been ice covered during the LIG. This places the GrIS evolution in the  
142 range of former model estimates during that period (e.g. Robinson et al., 2011; Born and  
143 Nisancioglu, 2012; Stone et al., 2013). Such scaling is in line with recent studies (e.g. van de  
144 Berg et al., 2013; Merz et al., 2014; Sjolte et al., 2014; Steen-Larsen et al., 2014) that put in  
145 question the high temperature of the central estimate reconstructed from the NEEM record.  
146 Precipitation rates for ice sheet forcing vary percentagewise as a function of the  $\delta^{18}\text{O}$  record.  
147 The AIS forcing is derived directly from the Antarctica Dome C record (EPICA community  
148 members, 2004), following again procedures described by Huybrechts (2002). Here  
149 precipitation changes are assumed proportional to the saturated water vapour pressure  
150 gradient relative to the temperature above the surface inversion layer. Furthermore, both ice  
151 sheet models are forced by changes in global sea-level stand based on the benthic deep-sea  
152 record of Lisiecki and Raymo (2005) for the GrIS and on a more recent sea-level  
153 reconstruction using Red Sea data (Grant et al., 2012) for the AIS, where the sea-level

154 changes are the dominant forcing. The chronology of the Red Sea record is expected to be  
155 more accurate since new dating techniques are applied (Grant et al., 2012). The impact of  
156 using another sea-level record for the GrIS simulation over the LIG is small, because of the  
157 largely land-based character of the ice sheet during that period. The AIS model is run at a  
158 horizontal resolution of 20 x 20 km instead of 10 km x 10 km (as in the standard LOVECLIM  
159 configuration and for the GrIS model) due to computational constraints for the relatively long  
160 duration of the LIG simulation.

161 To embed the dynamic GrIS simulation in the other NH boundary conditions, the geometric  
162 evolution of the GrIS overrides prescribed changes where Greenland ice is present. Therefore,  
163 the prescribed ice sheet evolution and associated FWF are not limited by the present-day  
164 configuration of the GrIS as in Loutre et al. (2014). The ice sheet evolution is illustrated in  
165 Figure 2 for the modelled GrIS embedded in the NH reconstruction (top) and for the modelled  
166 AIS (bottom). Ice volume evolution for the NH ice sheets and GrIS and AIS are given in  
167 Figure 3a and Figure 3c, respectively. The FWF from the dynamic GrIS and AIS (Figure 3d)  
168 replace the background freshwater flux from runoff over land calculated by the land model.

169 In our setup, the combined sea-level contributions from Antarctica and the NH (including  
170 Greenland) fall within the 67% confidence interval of probabilistic sea-level reconstructions  
171 (Kopp et al., 2009) for the first peak in sea-level contributions and the following period  
172 (~124-120 kyr BP). For both hemispheres, the final 20 m rise in sea-level at the onset of the  
173 LIG is however steeper and occurs 1~2 kyr earlier as compared to the reconstructions. When  
174 assuming a maximum contribution from glaciers ( $0.42 \pm 0.11$ ) and an additional estimate for  
175 thermal expansion of the ocean ( $0.4 \pm 0.3$ ) as given by Masson-Delmotte et al. (2013), the  
176 assumed ice sheet evolution in our setup reproduces well the average sea-level contribution  
177 between 125 and 120 kyr BP from the best estimate of Kopp et al. (2009), but it does not  
178 represent the multi-peak structure of global sea-level contribution during the LIG as suggested  
179 by Kopp et al. (2009, 2013). More details about the ice sheet and sea-level evolution can be  
180 found in a companion paper (Goelzer et al., 2016) that specifically deals with the sea-level  
181 contribution of the ice sheets during the LIG in a fully coupled model set-up.

## 182 **2.3 Initialisation**

183 The goal of our initialisation technique is to prepare a climate model state for the transient  
184 simulations starting at 135 kyr BP that exhibits a minimal coupling drift. Both the GrIS and

185 AIS models are integrated over the preceding glacial cycles and the entire LIG in stand-alone  
186 mode. The climate model is then initialized to a steady state with ice sheet boundary  
187 conditions, greenhouse gas (GHG) forcing and orbital parameters for the time of coupling  
188 (135 kyr BP). In this way, when LOVECLIM is integrated forward in time for transient  
189 experiments, the climate component is already relaxed to the ice sheet boundary conditions  
190 and exhibits a minimal model drift in unforced control experiments (not shown).

191

### 192 **3 Experimental setup**

193 All simulations are forced by time-dependent changes in GHG concentrations and insolation  
194 running from 135 kyr BP until 120 kyr BP (Figure 4). The radiative forcing associated with  
195 the reconstructed GHG levels (Petit et al., 1999; Pépin et al., 2001; Raynaud et al., 2005;  
196 Loulergue et al., 2008; Spahni et al., 2005) is below preindustrial values for most of this  
197 period and barely exceeds it at ~128 kyr BP. The changes in the distribution of insolation  
198 received by the Earth are dynamically computed from the changes in the orbital configuration  
199 (Berger, 1978) and represent the governing NH forcing during peak LIG conditions aside  
200 from evolving ice sheet boundary conditions. In the following, we will compare results of the  
201 reference experiment with all ice sheet boundary conditions evolving in time (Reference) to  
202 experiments in which the ice sheet boundary conditions are partially fixed to the pre-industrial  
203 configuration (Table 1). To disentangle the effects of the individual ice sheets, the  
204 experiments noGfwf (suppressed GrIS freshwater fluxes) and noAGfwf (suppressed FWF  
205 from both AIS and GrIS) are complemented by two predecessor experiments with fixed AIS  
206 and GrIS and evolving NH boundary conditions (noAG), as well as a climate experiment  
207 forced by insolation and GHG changes only with all ice sheet boundary conditions fixed  
208 (noIS). The latter two experiments correspond to the allLR and IGonly experiments from  
209 Loutre et al. (2014).

210

### 211 **4 Effect of GrIS and AIS on the temperature evolution at the onset of the LIG**

212 Including the forcing from the NH ice sheets in terms of configuration and FWF has been  
213 shown by Loutre et al. (2014) to be crucial to simulate the onset of the LIG temperature  
214 increase and its amplitude variations more in line with proxy records. This helps to partially  
215 overcome problems of EMICs (and general circulation models) to simulate the strong

216 temperature contrasts inferred from proxy reconstructions (Bakker et al., 2013; Lunt et al.,  
217 2013). The increased amplitude of temperature changes in our simulations is due to albedo  
218 and elevation changes in addition to the larger effect of the implied freshwater forcing from  
219 the NH ice sheets (Loutre et al., 2014). Here the Loutre et al. (2014) experiments are  
220 complemented with runs that additionally include changes in ice sheet configuration and FWF  
221 from the GrIS and AIS. We first discuss the effect of including these additional ice sheet  
222 boundary conditions. A specific focus on the FWF follows in section 5.

223 The temperature evolution (Figure 5) before 127 kyr BP is in both hemispheres strongly  
224 influenced by the ice sheet boundary conditions and in particular by the freshwater forcing  
225 from the ice sheets. The experiments including FWF from the NH ice sheets (Reference and  
226 noAG) clearly show temperature variations on the multi-millennial time scale in both  
227 hemispheres following variations in ice sheet freshwater input (cf. Figure 3). Differences in  
228 the temperature evolution between noAG and the reference experiment are small in the NH,  
229 where the additional freshwater flux from Greenland is small compared to the other sources.  
230 In the SH, by contrast, a large perturbation arises around 130 kyr BP, when FWF from the  
231 AIS peak. Global mean and hemispheric mean temperatures are similar in all runs after ~127  
232 kyr BP, when the ice sheets have largely reached their interglacial configuration and FWF are  
233 similar between the different experiments. An exception is the GrIS, which is retreating until  
234 ~120 kyr BP but accounts for only a small FWF contribution. The similarity of the results in  
235 the runs after ~127 kyr BP implies that the temporal memory of the response to ice sheet  
236 changes in the system is limited to the multi-centennial time scale, at least for the surface  
237 climate. The location of largest freshwater induced temperature variations in the NH is the  
238 North Atlantic between 40° N and 80° N. Here changes in the AMOC cause a perturbation of  
239 the northward oceanic heat transport and temperature changes, which are further amplified by  
240 sea ice-albedo and insulation feedbacks. Greenland experiences maximum warming in the  
241 reference experiment around 125 kyr BP of up to 2.7°C in the annual mean compared to the  
242 pre-industrial over remaining ice covered central Greenland. Here the temperature evolution  
243 is largely similar to the experiment with GrIS changes not accounted for (noAG), which  
244 exhibits a maximum warming of 2.4°C (Loutre et al., 2014). However, the summer warming  
245 reaches up to 10°C at the northern margin and even up to 14°C over southern margins over a  
246 then ice-free tundra (not shown). The strong warming in the ice sheet periphery is due to a  
247 combination of elevation changes and local albedo changes, confined to the immediate region  
248 of ice sheet lowering and retreat. In the SH, the largest temperature perturbations linked to



249 both NH and SH freshwater fluxes occur in the SO. The largest warming over the ice sheet  
250 itself is simulated over the WAIS (not shown) and is mainly a consequence of the local  
251 elevation changes as the ice sheet retreats. However, mainly due to the marine based character  
252 of the WAIS, albedo changes are much more limited compared to Greenland as the retreating  
253 ice sheet surface is mostly replaced by sea ice. Modelled temperature changes over the East  
254 Antarctic ice sheet (EAIS) have been compared to temperature reconstructions for four ice  
255 core locations (Figure 6). The reference experiment shows a more pronounced warming  
256 between 135 and 129.5 kyr BP compared to the experiments excluding Antarctic ice sheet  
257 changes (noAG and noIS). While the modelled warming still appears to be underestimated  
258 and delayed compared to the reconstructions, the reference simulation clearly improves the  
259 representation of the EAIS temperature evolution compared to experiments with fixed  
260 Antarctic boundary conditions.

261

## 262 **5 Role of ice sheet meltwater fluxes**

263 To study the role of the different freshwater contributions from the ice sheets in more detail  
264 and evaluate their importance for the climate evolution, we compare additional simulations  
265 where FWF from the GrIS and AIS are suppressed relative to the reference experiment  
266 (Figure 7). The ice sheet configuration (topography and albedo) remains unchanged in these  
267 experiments. The effect of AIS FWF can therefore be evaluated as the difference between  
268 noGfwf and noAGfwf, whereas the effect of GrIS FWF becomes apparent from comparing  
269 the reference simulation with noGfwf. The AIS FWF (Figure 7f) leads to considerable  
270 changes in the SH, but has very little impact on the NH temperature evolution (cf. Figure 5b).  
271 Conversely, variations in the NH (Figure 7a) and GrIS freshwater forcing on millennial time-  
272 scales imply temperature changes in the SH on a background of general LIG warming.

273 Differences between the experiments in the AMOC evolution (Figure 7b) are largely  
274 explained by whether FWF from the NH ice sheets and the GrIS are included or not. Here  
275 AMOC strength is calculated as the maximum value of the meridional overturning stream  
276 function below the Ekman layer in the Atlantic Ocean between 45° and 65° N. The effect of  
277 the FWF from the GrIS (cf. Reference and noGfwf in Figure 7b) is limited compared to the  
278 large impact of the general NH ice sheet forcing and consists of an additional weakening of  
279 the AMOC. It is most pronounced during periods of AMOC recovery and after 130 kyr BP,  
280 when melting of the GrIS beyond its present-day configuration sets in. Note that the simulated

281 evolution of AMOC strength in the reference experiment is in good agreement with paleo  
282 evidence based on  $\delta^{13}\text{C}$  data (Bauch et al., 2012) and in particular with a recent reconstruction  
283 based on chemical water tracers (Böhm et al., 2015). The timing of Heinrich Stadial 11 (~132  
284 kyr BP) and the variations in AMOC strength after that are well captured by our reference  
285 simulation, which gives independent credibility to our NH ice sheet reconstructions.

286 The evolution of NH sea ice area (Figure 7c) generally shows maxima at times of AMOC  
287 minima and vice versa and is closely linked to NH surface temperature variations (cf. Figure  
288 5b) by modifying the heat exchange between ocean and atmosphere. The largest sea ice area  
289 between 135 and 130 kyr BP is simulated in the reference experiment, which also exhibits the  
290 lowest AMOC strength of all experiments.

291 The situation in the SH is more complex as surface temperature and sea ice evolution are  
292 influenced both by freshwater forcing from the AIS as by the FWF in the NH. The AMOC  
293 variability gives rise to changes in the SH through the so-called interhemispheric see-saw  
294 effect (Stocker 1998). The SH begins to warm as the NH cools due to modified oceanic heat  
295 transport across the equator. Minima in SH temperature (cf. Figure 5c) and maxima in SH sea  
296 ice area (Figure 7d) are therefore associated with maxima in AMOC strength. The additional  
297 effect of including GrIS freshwater forcing is consequently also felt in a warmer SH with less  
298 sea ice formation. However, the influence of GrIS freshwater fluxes and consequential  
299 AMOC variations on the SH temperature appears to be mostly limited to the beginning of the  
300 experiment between ~135 and 131 kyr BP. It could be speculated that this is related to the  
301 larger extent of the SH sea ice in a colder climate, making the system more sensitive due to an  
302 increased potential for sea ice-albedo and insulation feedbacks. We also note that modelled  
303 periods of increased NH freshwater fluxes, reduced AMOC strength and higher SH  
304 temperatures are roughly in phase with periods of steeper increase in GHG concentrations (cf.  
305 Figure 4b), in line with evidence from marine sediment proxies that indicate that  $\text{CO}_2$   
306 concentration rose most rapidly when North Atlantic Deep Water shoaled (Ahn and Brook,  
307 2008). Since GHGs and NH freshwater fluxes are (independently) prescribed in our  
308 experiments, the described in-phase relationship lends further credibility to our NH ice sheet  
309 reconstruction.

310 The FWF from AIS melting (Figure 7f) increases the SO sea ice area (Figure 7d) by  
311 freshening and stratifying the upper ocean waters, which in turn leads to lower surface  
312 temperatures. In our experiments, the increased freshwater flux from the retreating AIS (cf.

313 noGfwf versus noAGfwf) between 131 and 129 kyr BP is in phase with a period of transient  
314 AMOC strengthening (Figure 7b), which leads to a combined effect of surface cooling and  
315 sea ice expansion in the SO.

316 The formation of AABW is strongly controlled by salinity and sea ice area (and therefore  
317 temperature) of the polar surface waters and hence by both Antarctic and indirectly by NH  
318 freshwater fluxes. Here the strength of AABW formation is calculated as the minimum value  
319 of the global meridional overturning stream function below the Ekman layer south of 60° S.  
320 The AABW formation (Figure 7e) is stronger for saltier and colder surface conditions and  
321 therefore strongest in case noAGfwf, where FWF are suppressed from the AIS (saltier) and  
322 the GrIS (colder). For a similar Antarctic freshwater forcing, the AABW formation is stronger  
323 for a larger SH sea ice area. Including Antarctic FWF leads to a generally weaker AABW  
324 formation as surface waters become fresher (cf. noGfwf versus noAGfwf). These  
325 relationships imply also that a stronger decrease in AABW formation, associated with  
326 decreased CO<sub>2</sub> uptake by the ocean can be found for periods of steeper increase in prescribed  
327 radiative forcing. Again, this appears to support consistency in timing between prescribed  
328 radiative and NH ice sheet forcing in our modelling.

329

## 330 **6 Temperature evolution in the Southern Hemisphere**

331 Millennial scale sea-surface temperature variations in the SH induced by NH freshwater  
332 fluxes are the strongest in the SO, where anomalies can be amplified by sea ice-albedo and  
333 insulation feedbacks. This is also the region that experiences the largest temperature change  
334 due to FWF from the AIS itself (not shown).

335 In order to study the effect of Antarctic FWF in more detail, we also analysed the oceanic  
336 temperature evolution south of 63°S (Figure 8). The effect of the AIS freshwater flux in the  
337 reference experiment (compare noAGfwf with reference) becomes visible in the sea surface  
338 temperature after 132 kyr BP (Figure 8a) as a cooling due to stratification and sea ice  
339 expansion (Figure 8c). At the same time, the subsurface ocean warms (Figure 8b) as heat is  
340 trapped under the stratified surface waters and expanding sea ice area. When the FWF decline  
341 towards the end of the AIS retreat around 128 kyr BP, sea ice retreats again and the heat is  
342 released to the atmosphere, where it generates an overshoot in SST compared to the  
343 experiment with constant Antarctic freshwater fluxes (noAGfwf). The largest effect of this  
344 heat buffering is found in winter in regions of strongest warming in the Bellingshausen Sea

345 and off the Gunnerus ridge adjacent to Dronning Maud Land. The maximum sea-ice extent in  
346 the SH (Figure 8c) occurs at the time of largest surface cooling at 129.5 kyr BP. This  
347 freshwater induced surface cooling at the onset of the LIG appears to be superficial and  
348 relatively short lived and of clearly different signature compared to e.g. the Antarctic cold  
349 reversal during the last deglaciation. The cooling event is indeed not recorded in our modelled  
350 temperature evolution over central East Antarctica, in line with a lack of its signature in  
351 Antarctic ice core records for that time period (Petit et al., 1999; EPICA community  
352 members, 2004). A sea ice expansion during Termination II together with an *oceanic* cold  
353 reversal around 129.5 kyr BP (Figure 8c) is however recorded in some deep-sea sediment  
354 cores, where the composition of planktonic diatoms suggests meltwater as the primary cause  
355 (Bianchi and Gersonde, 2002; Cortese and Abelmann, 2002).

356 As a further consequence, the timing of maximum annual mean surface air temperature  
357 (defined as MWT for Maximum Warmth Timing; Bakker et al., 2013) in the SO differs by  
358 several thousand years between experiments (Figure 9). Including Antarctic FWF leads to an  
359 earlier MWT (by up to 2 kyr) in large parts of the SO south of 60°S and in the central and  
360 eastern parts of the Atlantic sector of the SO up to 40°S (Figure 9d). Conversely, a later MWT  
361 (by up to 3 kyr) is found in the Indian and Pacific sectors of the SO north of 60°S when  
362 Antarctic FWF is accounted for (Figure 9d). In the reference experiment (Figure 9a) and  
363 noGfwf (Figure 9b), the MWT lies relatively homogeneously between -129 kyr and -128 kyr  
364 for the entire SO south of 45°S and coincides with the overshoot in SST after the peak input  
365 of Antarctic FWF. The observed changes of the MWT in the SO due to the additional  
366 Antarctic freshwater input can therefore in either way be understood as a shift towards the  
367 time when heat from the mid-depth ocean buffer is released to the surface.

368

## 369 **7 Discussion**

370 Despite remaining uncertainties in the timing of ice sheet retreat during Termination II, we  
371 find several lines of evidence in support of our ice sheet reconstructions and the associated  
372 climatic signatures. The NH ice sheet reconstruction shows some similarity with the IRD  
373 signal recorded in North Atlantic sediment cores (Kandiano et al., 2004; Oppo et al., 2006),  
374 while the simulated evolution of the AMOC strength (Figure 7a) is in good agreement with a  
375 recent reconstruction based on chemical water tracers (Böhm et al., 2015). The combination  
376 of NH and SH sourced freshwater forcing variations produces a stronger decrease in AABW

377 formation, associated with decreased CO<sub>2</sub> uptake by the ocean for periods of steeper increase  
378 in prescribed radiative forcing, in line with evidence from marine sediment proxies that  
379 indicate that CO<sub>2</sub> concentration rose most rapidly when North Atlantic Deep Water shoaled  
380 (Ahn and Brook, 2008). Reconstructing the NH ice sheet evolution during Termination II  
381 with the same method but using the Grant et al. (2012) sea-level record for comparison with  
382 Termination I has been shown to worsen agreement of the modelled climate with proxy  
383 reconstructions (Loutre et al., 2014).

384 Our modelling results furthermore suggest that the major AIS retreat from its glacial  
385 configuration could be constrained by an oceanic cold event recorded in several SO sediment  
386 cores around Antarctica (Bianchi and Gersonde, 2002; Cortese and Abelmann, 2002). As a  
387 schematic sensitivity test to uncertainties in the overall glacial AIS volume and retreat rate,  
388 we have performed one more experiment identical to the reference experiment except for  
389 Antarctic FWF scaled to 50% of their reference value. The resulting magnitude of the SO cold  
390 event and overshoot is lower but exhibits the same timing and spatial expression as in the  
391 reference case. The described mechanisms and effects can therefore be considered robust to  
392 differences in the magnitude of the freshwater flux, resulting from uncertainties in glacial ice  
393 volume or AIS retreat rate. Notably, the improved representation of the central East Antarctic  
394 temperature evolution in the model when including Antarctic ice sheet changes (Figure 6) is  
395 largely independent of the chosen freshwater forcing. This implies that changes in the  
396 geometry of the ice sheet and modified atmospheric circulation patterns are the cause for the  
397 stronger simulated temperature contrast.

398 The GrIS is generally assumed to have remained largely intact during the LIG (e.g. Robinson  
399 et al., 2011; Colville et al., 2011; Stone et al., 2013; NEEM community members, 2013) and  
400 indirect evidence of its freshwater contribution may be difficult to find due to the low  
401 amplitude compared to the other NH ice sheets. However, recent ice core reconstructions of  
402 the temperature evolution at the NEEM ice core site (NEEM community members, 2013)  
403 point to a late retreat with a peak sea-level contribution close to 120 kyr BP. The GrIS can be  
404 assumed to lose mass approximately as long as the temperature anomaly above the ice sheet  
405 remains above zero. Based on the NEEM record, which has been used as forcing time series  
406 in our stand-alone GrIS experiment, FWF from the GrIS peaks at ~125 kyr BP, but remains  
407 elevated until around 120 kyr BP above the steady state background flux of an ice sheet in  
408 equilibrium with the climate. The additional FWF from melting of the GrIS results in

409 relatively low temperatures over Southeast Greenland in response to a weakening of the  
410 AMOC (not shown). The interaction between GrIS meltwater fluxes and oceanic circulation  
411 hence give rise to a negative feedback on ice sheet retreat. This aspect could play an  
412 important role for the stability of the southern dome of the ice sheet and should be examined  
413 further with fully coupled climate-ice sheet simulations.

414 In general, the NH freshwater forcing leads to variations in the strength of the AMOC and  
415 North Atlantic cooling and additionally through the bipolar see-saw effect, to temperature  
416 changes in the SH. The only moment mid-depth ocean temperatures close to AIS grounding  
417 lines are above pre-industrial values in our experiments is during the oceanic cold reversal  
418 around 129.5 kyr BP, induced by anomalous FWF from the retreating AIS. During this  
419 period, SO mid-depth temperature anomalies relative to the pre-industrial reach up to 0.3 K,  
420 which could provide a positive but rather limited feedback on ice sheet retreat, similar to what  
421 has been suggested by Golledge et al. (2014) for meltwater pulse 1A during Termination I.  
422 However, the oceanic warming recorded in our model is not strong and the duration of the  
423 perturbation does not appear to be long enough for a sustained impact on the retreat of the ice  
424 sheet. Furthermore, the peak in freshwater flux appears when the ice sheet has already  
425 retreated considerably and WAIS grounding lines are located mostly on the continental  
426 shelves, more protected from the warm water build-up in the mid-depth ocean. A large-scale  
427 marine ice sheet retreat of the likely less vulnerable EAIS sectors (Mengel and Levermann,  
428 2014) appears particularly unlikely, given the atmospheric and oceanic forcing at the time  
429 apparent in our modelling results. However, in-depth studies of these interactions require  
430 detailed coupled simulations of the entire ocean-ice sheet system.

431 Despite aforementioned lines of evidence in support of the reconstructed NH ice sheet  
432 evolution, a limitation to our modelling approach is the rescaling of ice sheet retreat during  
433 Termination I, an attempt to address the sparseness of geomorphological field evidence for  
434 Termination II. An alternative approach would be to physically model all ice sheets together  
435 in one framework (e.g. de Boer et al. 2013), although spatial and temporal resolution of the  
436 models is a limiting factor in that specific case. A rigorous modelling approach like the latter  
437 could also help to prevent possible inconsistencies when combining ice sheet reconstructions  
438 from different approaches. Nevertheless, any modelling approach will ultimately be  
439 confronted with the same problem of scarce data for model validation during that period. The  
440 exclusion of climate feedbacks on ice sheet evolution of our present one-way coupled

441 modelling approach is a general limitation, which we have addressed in a separate study with  
442 a fully coupled model set-up (Goelzer et al., 2016).

443

## 444 **8 Conclusion**

445 We have presented a transient simulation of Termination II and the Last Interglacial period  
446 with realistic ice sheet boundary conditions from reconstructed NH ice sheets and detailed  
447 stand-alone simulations of the Greenland and Antarctic ice sheets. Our results show that the  
448 temperature evolution at the onset of the Last Interglacial was in both hemispheres  
449 considerably influenced by meltwater fluxes from the retreating ice sheets. While Antarctic  
450 freshwater fluxes lead to strong perturbations of the Southern Ocean, NH freshwater fluxes  
451 have an influence both on the Northern and SH temperature evolution through the oceanic  
452 see-saw effect. The importance of additional freshwater input from the GrIS during  
453 Termination II is small compared to the much larger fluxes from the other NH ice sheets and  
454 becomes more important only later during the Interglacial when it is the only remaining ice  
455 sheet contributing freshwater fluxes to the North Atlantic. In the SH, anomalous freshwater  
456 input from the AIS leads to an episode of surface freshening, increased stratification and sea  
457 ice cover and consequently reduced ocean heat loss to the atmosphere, with temporary heat  
458 build-up in the mid-depth ocean. We argue that the surface ocean cooling associated with this  
459 event may be used to constrain an early Antarctic retreat when matched with similar  
460 signatures evident in some deep-sea sediment cores from the Southern Ocean.

461 Our transient simulations confirm results from earlier studies that stress the importance of ice  
462 sheet boundary conditions for the climate evolution at the onset of the LIG. However, most of  
463 the freshwater induced changes remain visible for at most 1-2 kyr after cessation of the  
464 perturbations, indicative of a relative short memory of the (surface) climate system.  
465 Additional effects may arise from climate-ice sheet feedbacks not considered in the present  
466 model configuration, which should be investigated in fully-coupled experiments.

467

## 468 **Appendix A: Reconstruction of NH ice sheet forcing**

469 A direct reconstruction of NH ice sheet evolution during Termination II based on  
470 geomorphological data is not possible, due to the scarcity of field evidence that was mostly  
471 destroyed by the re-advancing ice sheets during the last glacial period. Therefore, a

472 reconstruction of Termination II is made by remapping the much better constrained ice sheet  
473 retreat of Termination I.

#### 474 **Ice extent during Termination I**

475 The evolution of the NH ice extent since the LGM was estimated based on published sources  
476 (Table A1) dating back to the time of the NH ice sheet studies of Zweck and Huybrechts  
477 (2003, 2005). For the large Laurentide and Eurasian ice sheets inferred ice extents are  
478 relatively well determined from geomorphological data and the reconstruction remains in  
479 good agreement with most recent sources (e.g. Hughes et al. 2016). For smaller ice sheets  
480 such as the European Alps previous modelled ice extent was used (Zweck and Huybrechts,  
481 2005).

482 For ice sheets with multiple sources of data the isochrones were merged using the most recent  
483 source when conflicts occurred (e.g. Dyke et al. (2002) instead of Dyke and Prest (1987) for  
484 the Innuitian ice sheet, Svendsen et al. (1999) instead of Andersen (1981) for the LGM  
485 maximum of the Eurasian ice sheet). The most recent source was then used as a mask of  
486 maximum ice extent for most recent isochrones of all sources. The only region, which  
487 experienced an advance in ice extent using this technique was the southern Cordilleran ice  
488 sheet according to the reconstruction of Clague and James (2002).

489 The INTCAL98 timescale of Stuiver et al. (1998) was used to convert radiocarbon dates to  
490 calendar years for the sources in Table A1. The retreat of the ice sheets between the LGM and  
491 PD was prescribed at 200 year resolution. Even for well-determined geomorphological  
492 observations, uncertainties in dating and from the conversion of radiocarbon to calendar years  
493 well exceed the 200 year temporal resolution used here. Figure A1 shows the deglaciation  
494 chronology reconstructed in this manner.

#### 495 **Ice sheet elevations during Termination I**

496 The NH ice sheets introduced significant changes to the surface topography of the region. As  
497 LOVECLIM1.3 has only 3 atmospheric height levels, details regarding topography are not  
498 strongly sensed. To include changes in surface topography in the model, parabolic profile ice  
499 sheets are constructed using the extents shown in Figure A1, neglecting isostatic adjustment  
500 (i.e. present-day surface elevation of the Earth's surface). The basal shear stress for the  
501 parabolic profile reconstruction is chosen so that the difference in ice volume between LGM  
502 and PD corresponds to 86 m of eustatic sea level change. With isostasy accounted for, a



503 similar elevation would result in an additional contribution of 24 m to a total equivalent  
504 eustatic sea level change of 110 m (cf. Zweck and Huybrechts, 2005). Using this procedure  
505 the maximum elevation of the Laurentide ice sheet is 3000 m near present-day Churchill in  
506 Hudson Bay, and the maximum elevation of the Eurasian ice sheet is 2600 m 100 km west of  
507 present-day Helsinki.

## 508 **Remapping Termination I to Termination II**

509 Remapping of the retreat during Termination I to Termination II is done using a benthic  $\delta^{18}\text{O}$   
510 record (Lisiecki and Raymo, 2005), assumed as an indicator of the global ice volume. In  
511 practice, the NH ice sheet configuration for a given time (and  $\delta^{18}\text{O}$  value) during Termination  
512 II is taken from a time during Termination I when the  $\delta^{18}\text{O}$  value had the same value. The  
513 LGM sea-level contribution of the NH ice sheets relative to the present day of -110 m  
514 translates into a similar magnitude for the penultimate glacial maximum (Lisiecki and Raymo,  
515 2005). The resulting NH ice volume evolution for Termination II is shown in Figure 3a.  
516 However, the method does not guarantee that the sea-level contribution of the reconstructed  
517 NH ice sheets closely follows the global ice volume curve. This is generally due to the  
518 mismatch between global ice volume and NH ice sheet reconstruction during Termination I,  
519 and in part related to the unconstrained contribution of other components (AIS, thermal  
520 expansion). Due to the assumed analogy, different configurations of the NH ice sheets (e.g.  
521 Obrochta et al., 2014) and different relative timing of NH and SH deglaciation between last  
522 and penultimate glaciation are not represented in these reconstructions. NH freshwater fluxes  
523 were estimated from the same method by using derived volume changes as input to a  
524 continental runoff routing model (Goelzer et al., 2012b) to identify the magnitude and  
525 location of meltwater fluxes to the ocean.

526  
527

## 528 **9 Acknowledgements**

529 We acknowledge support through the Belgian Federal Science Policy Office within its  
530 Research Programme on Science for a Sustainable Development under contract SD/CS/06A  
531 (iCLIPS). Computational resources have been provided by the supercomputing facilities of  
532 the Université catholique de Louvain (CISM/UCL) and the Consortium des Equipements de  
533 Calcul Intensif en Fédération Wallonie Bruxelles (CECI) funded by the Fond de la Recherche

534 Scientifique de Belgique (FRS-FNRS). We thank two anonymous reviewers and the editor for  
535 constructive comments and their follow-up of the manuscript.  
536

537 **10 References**

- 538 Ahn, J., and Brook, E.: Atmospheric CO<sub>2</sub> and climate on millennial time scales during the last  
539 glacial period, *Science*, 322, 83-85, doi: 10.1126/science.1160832 2008.
- 540 Andersen, B. G.: Late Weichselian ice sheets in Eurasia and Greenland, in: *The Last Great Ice*  
541 *Sheets*, edited by: Denton, G. H., and Hughes, T. J., Wiley Interscience, New York, 1 - 65,  
542 1981.
- 543 Bakker, P., Stone, E. J., Charbit, S., Gröger, M., Krebs-Kanzow, U., Ritz, S. P., Varma, V.,  
544 Khon, V., Lunt, D. J., Mikolajewicz, U., Prange, M., Renssen, H., Schneider, B., and Schulz,  
545 M.: Last interglacial temperature evolution &ndash; a model inter-comparison, *Clim.*  
546 *Past.*, 9, 605-619, doi:10.5194/cp-9-605-2013, 2013.
- 547 Barker, S., Knorr, G., Edwards, R. L., Parrenin, F., Putnam, A. E., Skinner, L. C., Wolff, E.,  
548 and Ziegler, M.: 800,000 Years of Abrupt Climate Variability, *Science*, 334, 347-351,  
549 doi:10.1126/science.1203580 2011.
- 550 Bauch, H. A., Kandiano, E. S., and Helmke, J. P.: Contrasting ocean changes between the  
551 subpolar and polar North Atlantic during the past 135 ka, *Geophys. Res. Lett.*, 39, L11604,  
552 doi:10.1029/2012GL051800, 2012.
- 553 Berger, A.: Long-term variations of daily insolation and Quaternary climatic changes, *Journal*  
554 *of Atmospheric Sciences*, 35, 2362-2367, doi:10.1175/1520-  
555 0469(1978)035<2362:LTVODI>2.0.CO;2, 1978.
- 556 Bianchi, C., and Gersonde, R.: The Southern Ocean surface between Marine Isotope Stages 6  
557 and 5d: Shape and timing of climate changes, *Palaeogeography, Palaeoclimatology,*  
558 *Palaeoecology*, 187, 151-177, doi:10.1016/S0031-0182(02)00516-3, 2002.
- 559 Bintanja, R., Van Oldenborgh, G. J., Drijfhout, S. S., Wouters, B., and Katsman, C. A.:  
560 Important role for ocean warming and increased ice-shelf melt in Antarctic sea-ice expansion,  
561 *Nat. Geosci.*, 6, 376-379, doi:10.1038/ngeo1767, 2013.
- 562 Böhm, E., Lippold, J., Gutjahr, M., Frank, M., Blaser, P., Antz, B., Fohlmeister, J., Frank, N.,  
563 Andersen, M. B., and Deininger, M.: Strong and deep Atlantic meridional overturning  
564 circulation during the last glacial cycle, *Nature*, 517, 73–76 doi:10.1038/nature14059, 2015.
- 565 Born, A., and Nisancioglu, K. H.: Melting of Northern Greenland during the last  
566 interglaciation, *Cryosphere*, 6, 1239-1250, doi:10.5194/tc-6-1239-2012, 2012.

567 Brovkin, V., Ganopolski, A., and Svirezhev, Y.: A continuous climate-vegetation  
568 classification for use in climate-biosphere studies, *Ecol. Model.*, 101, 251-261,  
569 doi:10.1016/S0304-3800(97)00049-5, 1997.

570 Capron, E., Govin, A., Stone, E. J., Masson-Delmotte, V., Mulitza, S., Otto-Bliesner, B.,  
571 Rasmussen, T. L., Sime, L. C., Waelbroeck, C., and Wolff, E. W.: Temporal and spatial  
572 structure of multi-millennial temperature changes at high latitudes during the Last  
573 Interglacial, *Quat. Sci. Rev.*, 103, 116-133, doi:10.1016/j.quascirev.2014.08.018, 2014.

574 Clague, J. J., and James, T. S.: History and isostatic effects of the last ice sheet in southern  
575 British Columbia, *Quat. Sci. Rev.*, 21, 71-87, doi:10.1016/s0277-3791(01)00070-1, 2002.

576 Colville, E. J., Carlson, A. E., Beard, B. L., Hatfield, R. G., Stoner, J. S., Reyes, A. V., and  
577 Ullman, D. J.: Sr-Nd-Pb Isotope Evidence for Ice-Sheet Presence on Southern Greenland  
578 During the Last Interglacial, *Science*, 333, 620-623, doi:10.1126/science.1204673, 2011.

579 Cortese, G., and Abelmann, A.: Radiolarian-based paleotemperatures during the last 160 kyr  
580 at ODP Site 1089 (Southern Ocean, Atlantic Sector), *Palaeogeography, Palaeoclimatology,*  
581 *Palaeoecology*, 182, 259-286, doi:10.1016/S0031-0182(01)00499-0, 2002.

582 de Boer, B., van de Wal, R. S. W., Lourens, L. J., Bintanja, R., and Reerink, T. J.: A  
583 continuous simulation of global ice volume over the past 1 million years with 3-D ice-sheet  
584 models, *Clim. Dyn.*, 41, 1365-1384, doi:10.1007/s00382-012-1562-2, 2013.

585 Driesschaert, E., Fichefet, T., Goosse, H., Huybrechts, P., Janssens, I., Mouchet, A.,  
586 Munhoven, G., Brovkin, V., and Weber, S.: Modeling the influence of Greenland ice sheet  
587 melting on the Atlantic meridional overturning circulation during the next millennia,  
588 *Geophys. Res. Lett.*, 34, 10707, doi:10.1029/2007GL029516, 2007.

589 Duplessy, J. C., Roche, D. M., and Kageyama, M.: The deep ocean during the last interglacial  
590 period, *Science*, 316, 89-91, doi:10.1126/science.1138582, 2007.

591 Dutton, A., and Lambeck, K.: Ice Volume and Sea Level During the Last Interglacial,  
592 *Science*, 337, 216-219, doi:10.1126/science.1205749, 2012.

593 Dyke, A. S., Andrews, J. T., Clark, P. U., England, J., Miller, G. H., Shaw, J., and Veillette, J.  
594 J.: The Laurentide and Innuitian ice sheets during the Last Glacial Maximum, *Quat. Sci. Rev.*,  
595 21, 9-31, doi:10.1016/S0277-3791(01)00095-6, 2002.

596 Dyke, A. S., and Prest, V. K.: Late Wisconsinan and Holocene history of the Laurentide Ice  
597 Sheet, *Géog. Phys. Quat.*, 41, 237 - 263, doi:10.7202/032681ar, 1987.

598 EPICA community members: Eight glacial cycles from an Antarctic ice core, *Nature*, 429,  
599 623-628, doi:10.1038/Nature02599, 2004.

600 Fürst, J. J., Goelzer, H., and Huybrechts, P.: Ice-dynamic projections of the Greenland ice  
601 sheet in response to atmospheric and oceanic warming, *The Cryosphere*, 9, 1039-1062,  
602 doi:10.5194/tc-9-1039-2015, 2015.

603 Goelzer, H., Huybrechts, P., Loutre, M. F., Goosse, H., Fichet, T., and Mouchet, A.: Impact  
604 of Greenland and Antarctic ice sheet interactions on climate sensitivity, *Clim. Dyn.*, 37, 1005-  
605 1018, doi:10.1007/s00382-010-0885-0, 2011.

606 Goelzer, H., Huybrechts, P., Raper, S. C. B., Loutre, M. F., Goosse, H., and Fichet, T.:  
607 Millennial total sea level commitments projected with the Earth system model of intermediate  
608 complexity LOVECLIM, *Environ. Res. Lett.*, 7, doi:10.1088/1748-9326/7/4/045401, 2012a.

609 Goelzer, H., Janssens, I., Nemeč, J., and Huybrechts, P.: A dynamic continental runoff  
610 routing model applied to the last Northern Hemisphere deglaciation, *Geosci. Model Dev.*, 5,  
611 599-609, doi:10.5194/gmd-5-599-2012, 2012b.

612 Goelzer, H., Huybrechts, P., Loutre, M.-F., and Fichet, T.: Last Interglacial climate and sea-  
613 level evolution from a coupled ice sheet-climate model, *Clim. Past. Discuss.*, in review,  
614 doi:10.5194/cp-2015-175, 2016.

615 Golledge, N. R., Menviel, L., Carter, L., Fogwill, C. J., England, M. H., Cortese, G., and  
616 Levy, R. H.: Antarctic contribution to meltwater pulse 1A from reduced Southern Ocean  
617 overturning, *Nature Communications*, 5, doi:10.1038/ncomms6107, 2014.

618 Goosse, H., and Fichet, T.: Importance of ice-ocean interactions for the global ocean  
619 circulation: A model study, *J. Geophys. Res.*, 104, 23337-23355, doi:10.1029/1999JC900215,  
620 1999.

621 Goosse, H., Brovkin, V., Fichet, T., Haarsma, R., Huybrechts, P., Jongma, J., Mouchet, A.,  
622 Selten, F., Barriat, P.-Y., Campin, J.-M., Deleersnijder, E., Driesschaert, E., Goelzer, H.,  
623 Janssens, I., Loutre, M. F., Morales Maqueda, M. A., Opsteegh, T., Mathieu, P.-P.,  
624 Munhoven, G., Pettersson, E. J., Renssen, H., Roche, D. M., Schaeffer, M., Tartinville, B.,  
625 Timmermann, A., and Weber, S. L.: Description of the Earth system model of intermediate

626 complexity LOVECLIM version 1.2, *Geosci. Model Dev.*, 3, 603-633, doi:10.5194/gmd-3-  
627 603-2010, 2010.

628 Govin, A., Braconnot, P., Capron, E., Cortijo, E., Duplessy, J. C., Jansen, E., Labeyrie, L.,  
629 Landais, A., Marti, O., Michel, E., Mosquet, E., Risebrobakken, B., Swingedouw, D., and  
630 Waelbroeck, C.: Persistent influence of ice sheet melting on high northern latitude climate  
631 during the early Last Interglacial, *Clim. Past.*, 8, 483-507, doi:10.5194/cp-8-483-2012, 2012.

632 Grant, K. M., Rohling, E. J., Bar-Matthews, M., Ayalon, A., Medina-Elizalde, M., Ramsey,  
633 C. B., Satow, C., and Roberts, A. P.: Rapid coupling between ice volume and polar  
634 temperature over the past 150,000 years, *Nature*, 1-4, doi:10.1038/nature11593, 2012.

635 Greve, R., Saito, F., and Abe-Ouchi, A.: Initial results of the SeaRISE numerical experiments  
636 with the models SICOPOLIS and IcIES for the Greenland ice sheet, *Ann. Glaciol.*, 52, 23-30,  
637 doi:10.3189/172756411797252068, 2011.

638 Holden, P., Edwards, N. R., Wolff, E., Lang, N., Singarayer, J., Valdes, P., and Stocker, T.:  
639 Interhemispheric coupling, the West Antarctic Ice Sheet and warm Antarctic interglacials,  
640 *Clim. Past.*, 6, 431-443, doi:10.5194/cp-6-431-2010, 2010.

641 Hughes, A. L. C., Gyllencreutz, R., Lohne, Ø. S., Mangerud, J., and Svendsen, J. I.: The last  
642 Eurasian ice sheets – a chronological database and time-slice reconstruction, *DATED-1*,  
643 *Boreas*, 45, 1-45, doi:10.1111/bor.12142, 2016.

644 Huybrechts, P.: A 3-D model for the Antarctic Ice Sheet: a sensitivity study on the glacial-  
645 interglacial contrast, *Clim. Dyn.*, 5, 79-92, doi:10.1007/BF00207423, 1990.

646 Huybrechts, P.: Sea-level changes at the LGM from ice-dynamic reconstructions of the  
647 Greenland and Antarctic ice sheets during the glacial cycles, *Quat. Sci. Rev.*, 21, 203-231,  
648 doi:10.1016/S0277-3791(01)00082-8, 2002.

649 Kandiano, E. S., Bauch, H. A., and Müller, A.: Sea surface temperature variability in the  
650 North Atlantic during the last two glacial–interglacial cycles: comparison of faunal, oxygen  
651 isotopic, and Mg/Ca-derived records, *Palaeogeography, Palaeoclimatology, Palaeoecology*,  
652 204, 145-164, doi:10.1016/S0031-0182(03)00728-4, 2004.

653 Kopp, R. E., Simons, F. J., Mitrovica, J. X., Maloof, A. C., and Oppenheimer, M.:  
654 Probabilistic assessment of sea level during the last interglacial stage, *Nature*, 462, 863-867,  
655 doi:10.1038/nature08686, 2009.

656 Kopp, R. E., Simons, F. J., Mitrovica, J. X., Maloof, A. C., and Oppenheimer, M.: A  
657 probabilistic assessment of sea level variations within the last interglacial stage, *Geophys. J.*  
658 *Int.*, 193, 711-716, doi:10.1093/gji/ggt029, 2013.

659 Landvik, J. Y., Bondevik, S., Elverhøi, A., Fjeldskaar, W., Mangerud, J., Salvigsen, O.,  
660 Siegert, M. J., Svendsen, J. I., and Vorren, T. O.: The Last Glacial Maximum of Svalbard and  
661 the Barents Sea area: ice sheet extent and configuration, *Quat. Sci. Rev.*, 17, 43-75,  
662 doi:10.1016/S0277-3791(97)00066-8, 1998.

663 Langebroek, P. M., and Nisancioglu, K. H.: Simulating last interglacial climate with  
664 NorESM: role of insolation and greenhouse gases in the timing of peak warmth, *Clim. Past.*,  
665 10, 1305-1318, doi:10.5194/cp-10-1305-2014, 2014.

666 Letréguilly, A., Huybrechts, P., and Reeh, N.: Steady-state characteristics of the Greenland  
667 ice sheet under different climates, *J. Glaciol.*, 37, 149-157, 1991.

668 Lisiecki, L. E., and Raymo, M. E.: A Pliocene-Pleistocene stack of 57 globally distributed  
669 benthic delta O-18 records, *Paleoceanography*, 20, 17, doi:10.1029/2004pa001071, 2005.

670 Loulergue, L., Schilt, A., Spahni, R., Masson-Delmotte, V., Blunier, T., Lemieux, B.,  
671 Barnola, J.-M., D. Raynaud, Stocker, T. F., and Chappellaz, J.: Orbital and millennial-scale  
672 features of atmospheric CH<sub>4</sub> over the past 800,000 years, *Nature*, 453, 383-386,  
673 doi:10.1038/nature06950, 2008.

674 Loutre, M. F., Fichet, T., Goosse, H., Huybrechts, P., Goelzer, H., and Capron, E.: Factors  
675 controlling the last interglacial climate as simulated by LOVECLIM1.3, *Clim. Past.*, 10,  
676 1541-1565, doi:10.5194/cp-10-1541-2014, 2014.

677 Lunt, D. J., Abe-Ouchi, A., Bakker, P., Berger, A., Braconnot, P., Charbit, S., Fischer, N.,  
678 Herold, N., Jungclauss, J. H., Khon, V. C., Krebs-Kanzow, U., Langebroek, P. M., Lohmann,  
679 G., Nisancioglu, K., Otto-Bliesner, B., Park, W., Pfeiffer, M., Phipps, S. J., Prange, M.,  
680 Rachmayani, R., Renssen, H., Rosenbloom, N., Schneider, B., Stone, E. J., Takahashi, K.,  
681 Wei, W., Yin, Q., and Zhang, Z. S.: A multi-model assessment of last interglacial  
682 temperatures, *Clim. Past.*, 9, 699-717, doi:10.5194/cp-9-699-2013, 2013.

683 Mangerud, J., Astakhov, V., and Svendsen, J. I.: The extent of the Barents-Kara Ice Sheet  
684 during the Last Glacial Maximum, *Quat. Sci. Rev.*, 21, 111-119, doi:10.1016/s0277-  
685 3791(01)00088-9, 2002.

686 Marino, G., Rohling, E. J., Rodriguez-Sanz, L., Grant, K. M., Heslop, D., Roberts, A. P.,  
687 Stanford, J. D., and Yu, J.: Bipolar seesaw control on last interglacial sea level, *Nature*, 522,  
688 197-201, doi:10.1038/nature14499, 2015.

689 Masson-Delmotte, V., Buiron, D., Ekaykin, A., Frezzotti, M., Gallée, H., Jouzel, J., Krinner,  
690 G., Landais, A., Motoyama, H., Oerter, H., Pol, K., Pollard, D., Ritz, C., Schlosser, E., Sime,  
691 L. C., Sodemann, H., Stenni, B., Uemura, R., and Vimeux, F.: A comparison of the present  
692 and last interglacial periods in six Antarctic ice cores, *Clim. Past.*, 7, 397-423,  
693 doi:10.5194/cp-7-397-2011, 2011.

694 Masson-Delmotte, V., Schulz, M., Abe-Ouchi, A., Beer, J., Ganopolski, A., González Rouco,  
695 J., Jansen, E., Lambeck, K., Luterbacher, J., Naish, T., Osborn, T., Otto-Bliesner, B., T.  
696 Quinn, R. R., M. Rojas, X. S., and Timmermann, A.: Information from paleoclimate archives,  
697 in: *Climate Change 2013: The Physical Science Basis. Contribution of Working Group I to*  
698 *the Fifth Assessment Report of the Intergovernmental Panel on Climate Change*, edited by:  
699 Stocker, T. F., Qin, D., Plattner, G.-K., Tignor, M., Allen, S. K., Boschung, J., Nauels, A.,  
700 Xia, Y., Bex, V., and Midgley, P. M., Cambridge University Press, , Cambridge, United  
701 Kingdom and New York, NY, USA, 383-464, 2013.

702 Mayewski, P., Denton, G., and Hughes, T.: Late Wisconsin Ice Sheets in North America, in:  
703 *The Last Great Ice Sheets*, edited by: Denton, G., and Hughes, T., Wiley Interscience, New  
704 York, 67-178, 1981.

705 Mengel, M., and Levermann, A.: Ice plug prevents irreversible discharge from East  
706 Antarctica, *Nature Climate Change*, 4, 451-455, doi:10.1038/nclimate2226, 2014.

707 Menviel, L., Timmermann, A., Timm, O. E., and Mouchet, A.: Deconstructing the Last  
708 Glacial termination: the role of millennial and orbital-scale forcings, *Quat. Sci. Rev.*, 30,  
709 1155-1172, doi:10.1016/j.quascirev.2011.02.005, 2011.

710 Merz, N., Born, A., Raible, C. C., Fischer, H., and Stocker, T. F.: Dependence of Eemian  
711 Greenland temperature reconstructions on the ice sheet topography, *Clim. Past*, 10, 1221-  
712 1238, doi:10.5194/cp-10-1221-2014, 2014.

713 NEEM community members: Eemian interglacial reconstructed from a Greenland folded ice  
714 core, *Nature*, 493, 489-494, doi:10.1038/nature11789, 2013.



715 Obrochta, S. P., Crowley, T. J., Channell, J. E. T., Hodell, D. A., Baker, P. A., Seki, A., and  
716 Yokoyama, Y.: Climate variability and ice-sheet dynamics during the last three glaciations,  
717 *Earth Planet. Sci. Lett.*, 406, 198-212, doi:10.1016/j.epsl.2014.09.004, 2014.

718 Oppo, D. W., McManus, J. F., and Cullen, J. L.: Evolution and demise of the Last Interglacial  
719 warmth in the subpolar North Atlantic, *Quat. Sci. Rev.*, 25, 3268-3277,  
720 doi:10.1016/j.quascirev.2006.07.006, 2006.

721 Opsteegh, J. D., Haarsma, R. J., Selten, F. M., and Kattenberg, A.: ECBILT: a dynamic  
722 alternative to mixed boundary conditions in ocean models, *Tellus*, 50, 348-367,  
723 doi:10.1034/j.1600-0870.1998.t01-1-00007.x, 1998.

724 Pépin, L., Raynaud, D., Barnola, J. M., and Loutre, M. F.: Hemispheric roles of climate  
725 forcings during glacial-interglacial transitions as deduced from the Vostok record and LLN-  
726 2D model experiments, *J. Geophys. Res. [Atmos.]*, 106, 31885-31892,  
727 doi:10.1029/2001jd900117, 2001.

728 Petit, J.-R., Jouzel, J., Raynaud, D., Barkov, N. I., Barnola, J.-M., Basile, I., Bender, M.,  
729 Chappellaz, J., Davis, M. E., Delaygue, G., Delmotte, M., Kotlyakov, V. M., Legrand, M.,  
730 Lipenkov, V. Y., Lorius, C., Pepin, L., Ritz, C., Saltzman, E., and Stievenard, M.: Climate  
731 and atmospheric history of the past 420,000 years from the Vostok ice core, *Antarctica*,  
732 *Nature*, 399, 429-436, doi:10.1038/20859, 1999.

733 Raynaud, D., Barnola, J. M., Souchez, R., Lorrain, R., Petit, J. R., Duval, P., and Lipenkov,  
734 V. Y.: Palaeoclimatology - The record for marine isotopic stage 11, *Nature*, 436, 39-40,  
735 doi:10.1038/43639b, 2005.

736 Robinson, A., Calov, R., and Ganopolski, A.: Greenland ice sheet model parameters  
737 constrained using simulations of the Eemian Interglacial, *Clim. Past.*, 7, 381-396,  
738 doi:10.5194/cp-7-381-2011, 2011.

739 Sánchez Goñi, M. F., Bakker, P., Desprat, S., Carlson, A. E., Van Meerbeeck, C. J., Peyron,  
740 O., Naughton, F., Fletcher, W. J., Eynaud, F., Rossignol, L., and Renssen, H.: European  
741 climate optimum and enhanced Greenland melt during the Last Interglacial, *Geology*, 40,  
742 627-630, doi:10.1130/G32908.1 2012.

743 Sjolte, J., and Hoffmann, G.: Modelling stable water isotopes in monsoon precipitation during  
744 the previous interglacial, *Quat. Sci. Rev.*, 85, 119-135, doi:10.1016/j.quascirev.2013.12.006,  
745 2014.

746 Spahni, R., Chappellaz, J., Stocker, T. F., Loulerge, L., Hausammann, G., Kawamura, K.,  
747 Flückiger, J., Schwander, J., Raynaud, D., Masson-Delmotte, V., and Jouzel, J.: Atmospheric  
748 methane and nitrous oxide of the late Pleistocene from Antarctic ice cores, *Science*, 310,  
749 1317-1321, doi:10.1126/science.1120132 2005.

750 Steen-Larsen, H. C., Masson-Delmotte, V., Hirabayashi, M., Winkler, R., Satow, K., Prié, F.,  
751 Bayou, N., Brun, E., Cuffey, K. M., Dahl-Jensen, D., Dumont, M., Guillevic, M., Kipfstuhl,  
752 S., Landais, A., Popp, T., Risi, C., Steffen, K., Stenni, B., and Sveinbjörnsdóttir, A. E.: What  
753 controls the isotopic composition of Greenland surface snow?, *Clim. Past.*, 10, 377-392,  
754 doi:10.5194/cp-10-377-2014, 2014.

755 Stocker, T. F.: The Seesaw Effect, *Science*, 282, 61-62, doi:10.1126/science.282.5386.61,  
756 1998.

757 Stocker, T. F., and Johnsen, S. J.: A minimum thermodynamic model for the bipolar seesaw,  
758 *Paleoceanography*, 18, 1087, doi:10.1029/2003PA000920, 2003.

759 Stone, E. J., Lunt, D. J., Annan, J. D., and Hargreaves, J. C.: Quantification of the Greenland  
760 ice sheet contribution to Last Interglacial sea level rise, *Clim. Past.*, 9, 621-639,  
761 doi:10.5194/cp-9-621-2013, 2013.

762 Stuiver, M., Reimer, P. J., Bard, E., Beck, J. W., Burr, G. S., Hughen, K. A., Kromer, B.,  
763 McCormac, G., van der Plicht, J., and Spurk, M.: INTCAL98 radiocarbon age calibration,  
764 24,000-0 cal BP, *Radiocarbon*, 40, 1041-1083, 1998.

765 Svendsen, J. I., Alexanderson, H., Astakhov, V. I., Demidov, I., Dowdeswell, J. A., Funder,  
766 S., Gataullin, V., Henriksen, M., Hjort, C., Houmark-Nielsen, M., Hubberten, H. W.,  
767 Ingolfsson, O., Jakobsson, M., Kjær, K. H., Larsen, E., Lokrantz, H., Lunkka, J. P., Lyså, A.,  
768 Mangerud, J., Matiouchkov, A., Murray, A., Möller, P., Niessen, F., Nikolskaya, O., Polyak,  
769 L., Saarnisto, M., Siegert, C., Siegert, M. J., Spielhagen, R., and Stein, R.: Late Quaternary  
770 ice sheet history of northern Eurasia, *Quat. Sci. Rev.*, 23, 1229-1271,  
771 doi:10.1016/j.quascirev.2003.12.008, 2004.

772 Svendsen, J. I., Astakhov, V. I., Bolshiyarov, D. Y., Demidov, I., Dowdeswell, J. A.,  
773 Gataullin, V., Hjort, C., Hubberten, H. W., Larsen, E., Mangerud, J., Melles, M., Möller, P.,  
774 Saarnisto, M., and Siegert, M. J.: Maximum extent of the Eurasian ice sheets in the Barents  
775 and Kara Sea region during the Weichselian, *Boreas*, 28, 234-242, doi:10.1111/j.1502-  
776 3885.1999.tb00217.x, 1999.

777 Swingedouw, D., Fichefet, T., Huybrechts, P., Goosse, H., Driesschaert, E., and Loutre, M.  
778 F.: Antarctic ice-sheet melting provides negative feedbacks on future climate warming,  
779 *Geophys. Res. Lett.*, 35, L17705, doi:10.1029/2008GL034410, 2008.

780 Turney, C. S. M., and Jones, R. T.: Does the Agulhas Current amplify global temperatures  
781 during super-interglacials?, *J. Quat. Sci.*, 25, 839-843, doi:10.1002/jqs.1423, 2010.

782 van de Berg, W. J., van den Broeke, M. R., van Meijgaard, E., and Kaspar, F.: Importance of  
783 precipitation seasonality for the interpretation of Eemian ice core isotope records from  
784 Greenland, *Clim. Past.*, 9, 1589-1600, doi:10.5194/cp-9-1589-2013, 2013.

785 Zweck, C., and Huybrechts, P.: Modeling the marine extent of northern hemisphere ice sheets  
786 during the last glacial cycle, *Ann. Glaciol.*, 37, 173-180, doi:10.3189/172756403781815870,  
787 2003.

788 Zweck, C., and Huybrechts, P.: Modeling of the northern hemisphere ice sheets during the  
789 last glacial cycle and glaciological sensitivity, *J. Geophys. Res.*, 110, D07103,  
790 doi:10.1029/2004JD005489, 2005.

791

792

793

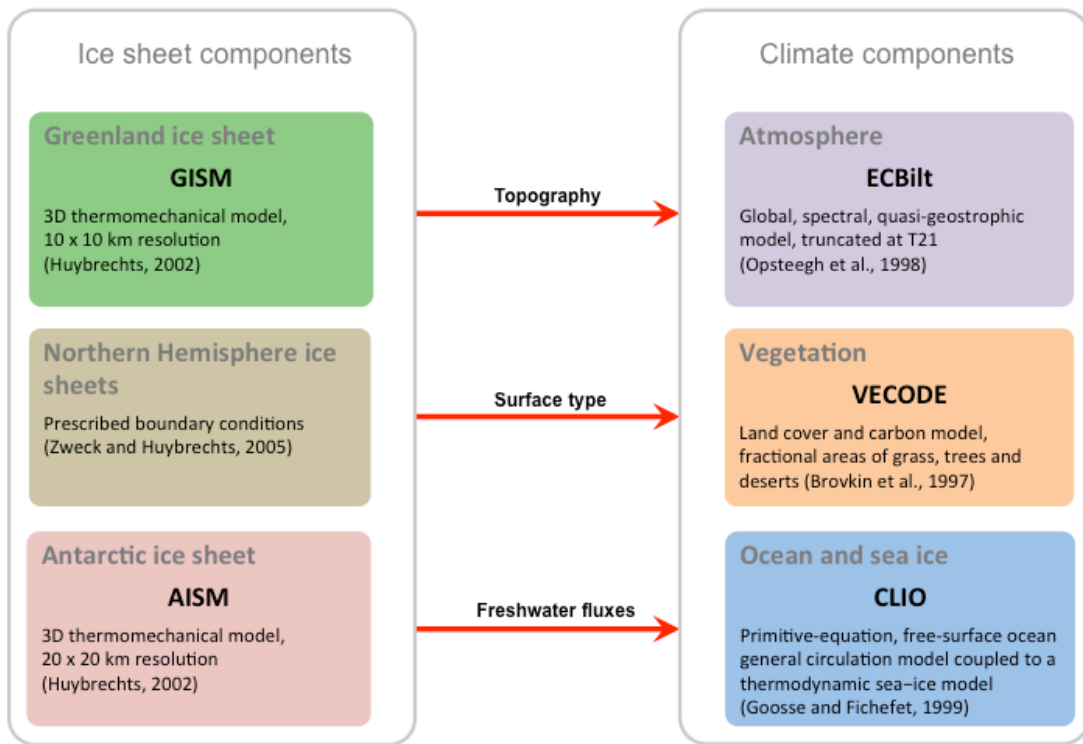
794 **11 Tables**

795

796 **Table 1: Matrix of all experiments and the respective ice sheet components that evolve in time (yes) or are**  
 797 **fixed (no). In the latter case, freshwater fluxes (FWF, grey) are kept constant and topography and surface**  
 798 **albedo are fixed to the preindustrial configuration.**

EXP	topo NH	FWF NH	topo GrIS	FWF GrIS	topo AIS	FWF AIS
Reference	yes	yes	yes	yes	yes	yes
noGfwf	yes	yes	yes	no	yes	yes
noAGfwf	yes	yes	yes	no	yes	no
noAG	yes	yes	no	no	no	no
noIS	no	no	no	no	no	no

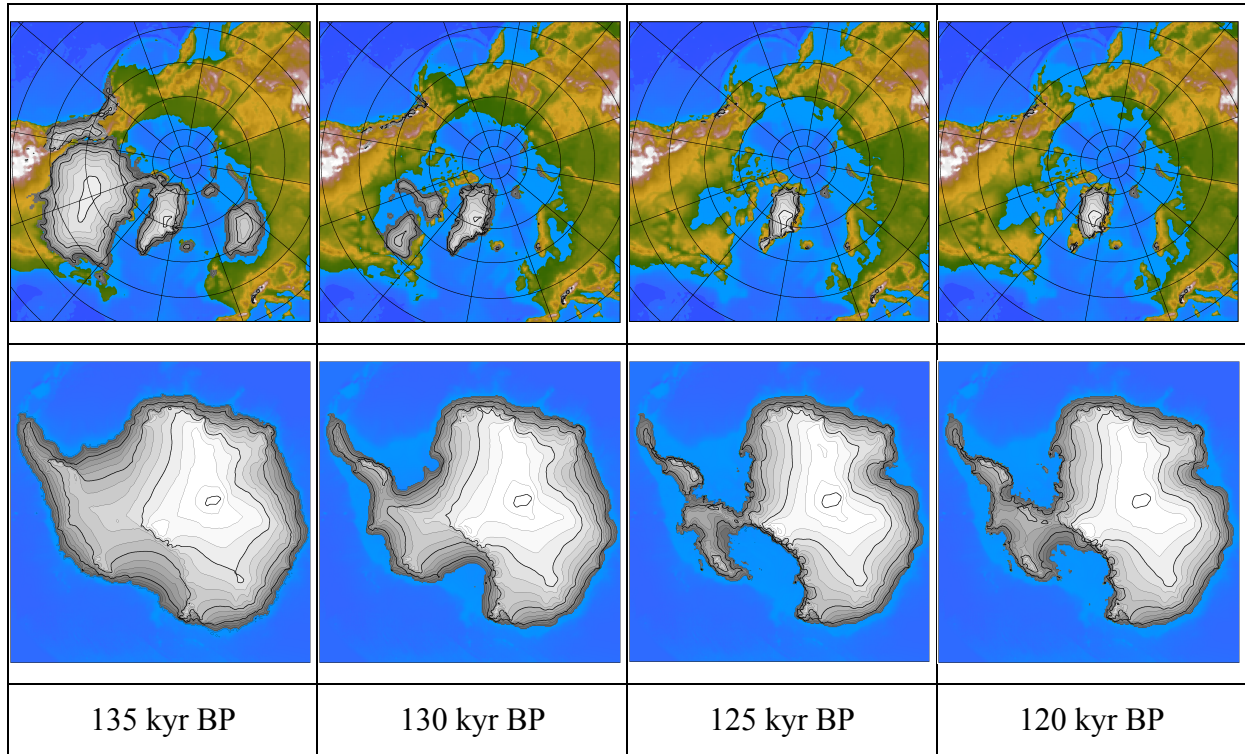
799



801

802 **Figure 1: LOVECLIM model setup for the present study including prescribed ice sheet boundary**  
 803 **conditions from the Northern Hemisphere, Greenland and Antarctic ice sheets.**

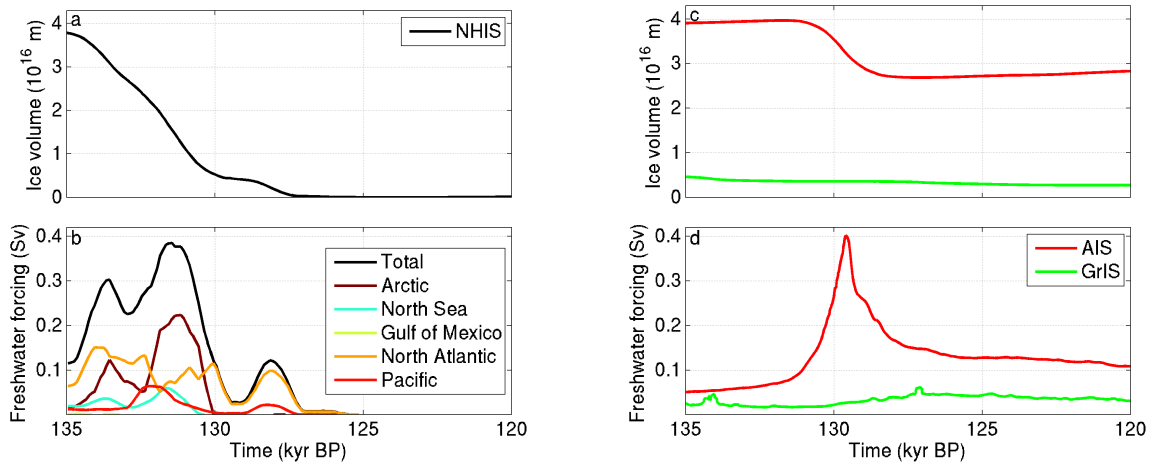
804



806 **Figure 2: Evolution of reconstructed Northern Hemisphere ice sheets and embedded modelled GrIS (top)**  
 807 **and modelled AIS (bottom) used as boundary conditions for the climate model.**

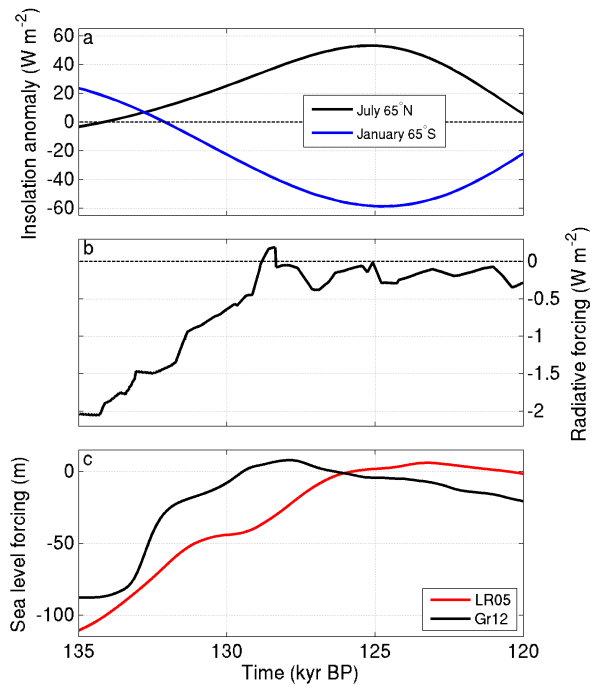
808

809

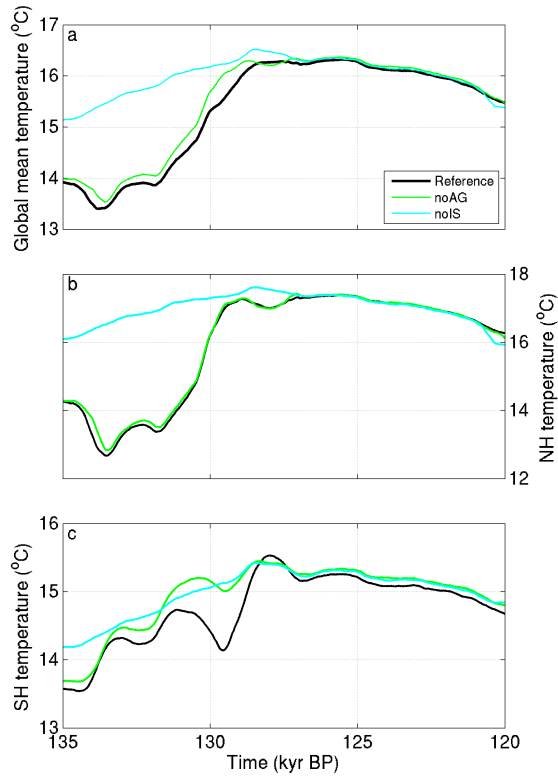


810 **Figure 3: Reconstructed ice volume (a, c) and freshwater forcing (b, d) from the NH ice sheets (left) and**  
 811 **from the GrIS and AIS (right). See Goelzer et al. (2012b) for definition of oceanic basins in panel b.**

812



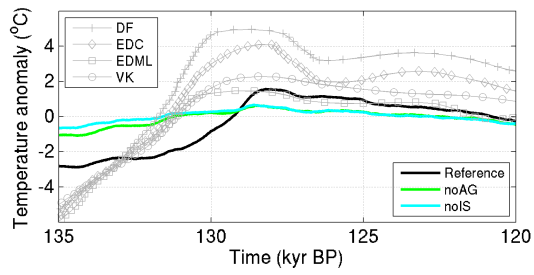
813 **Figure 4: Prescribed model forcings. (a) Average monthly insolation anomaly relative to the pre-industrial**  
 814 **at 65° North in July (black) and 65° South in January (blue). (b) combined radiative forcing anomaly of**  
 815 **prescribed greenhouse gas concentrations (CO<sub>2</sub>, CH<sub>4</sub>, N<sub>2</sub>O ) relative to the pre-industrial. (c) sea-level**  
 816 **forcing for the ice sheet components derived from either oceanic δ<sup>18</sup>O data (Lisiecki and Raymo, 2005,**  
 817 **red) scaled to a global sea-level contrast between LGM and present day of 130 m or derived from a Red**  
 818 **Sea relative sea-level record (Grant et al. 2012, black).**  
 819



821 **Figure 5: Evolution of global mean (a), northern (b) and southern (c) hemispheric mean surface**  
 822 **temperature for experiments with different ice sheet forcing included. Curves are smoothed with a**  
 823 **running mean of 200 years for better comparison.**

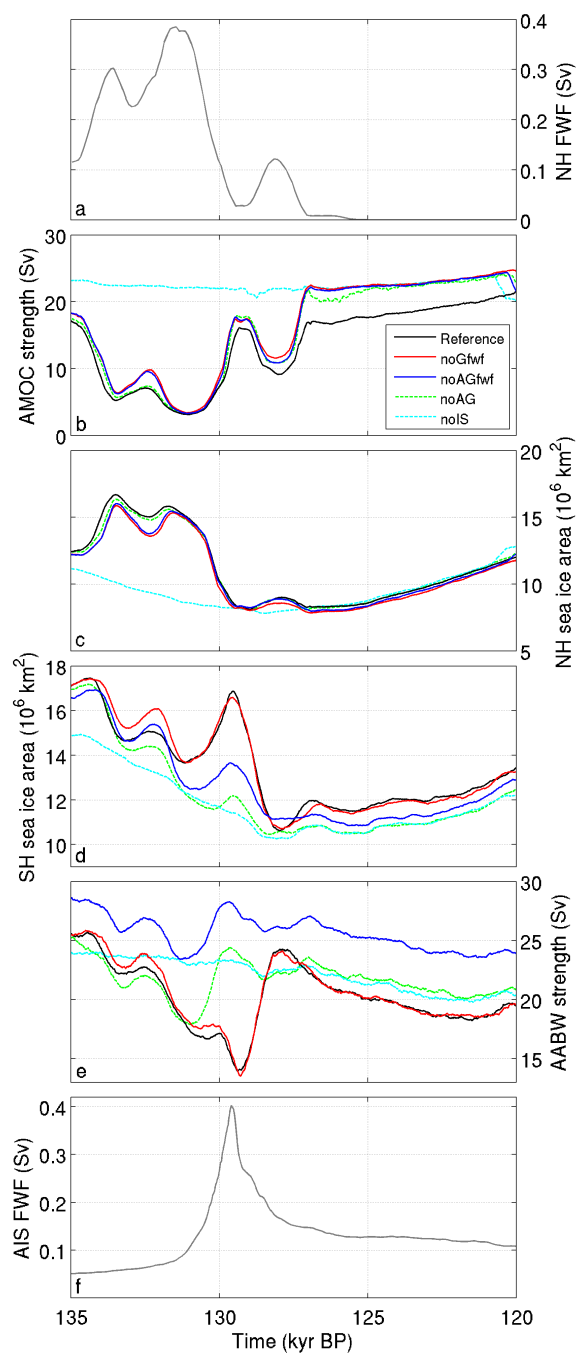
824



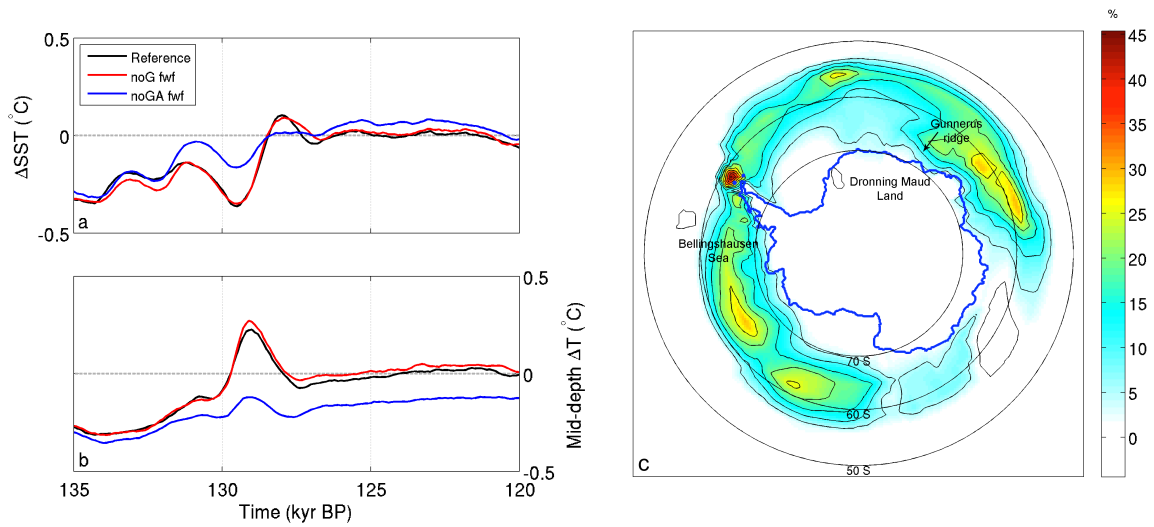


825

826 **Figure 6: Comparison of modelled East Antarctic temperature evolution with reconstructed temperature**  
 827 **changes at deep ice core sites. Modelled temperature anomalies are averaged over a region 72° - 90° S and**  
 828 **0° - 150° E. Ice core temperature reconstructions for the sites EPICA Dronning Maud Land (EDML,**  
 829 **75°00' S, 00°04' E), Dome Fuji (DF, 77°19' S, 39°40' E), Vostok (VK, 78°28' S, 106°48' E) and EPICA**  
 830 **Dome C (EDC, 75°06' S, 123°21' E) are from Masson-Delmotte et al. (2011).**



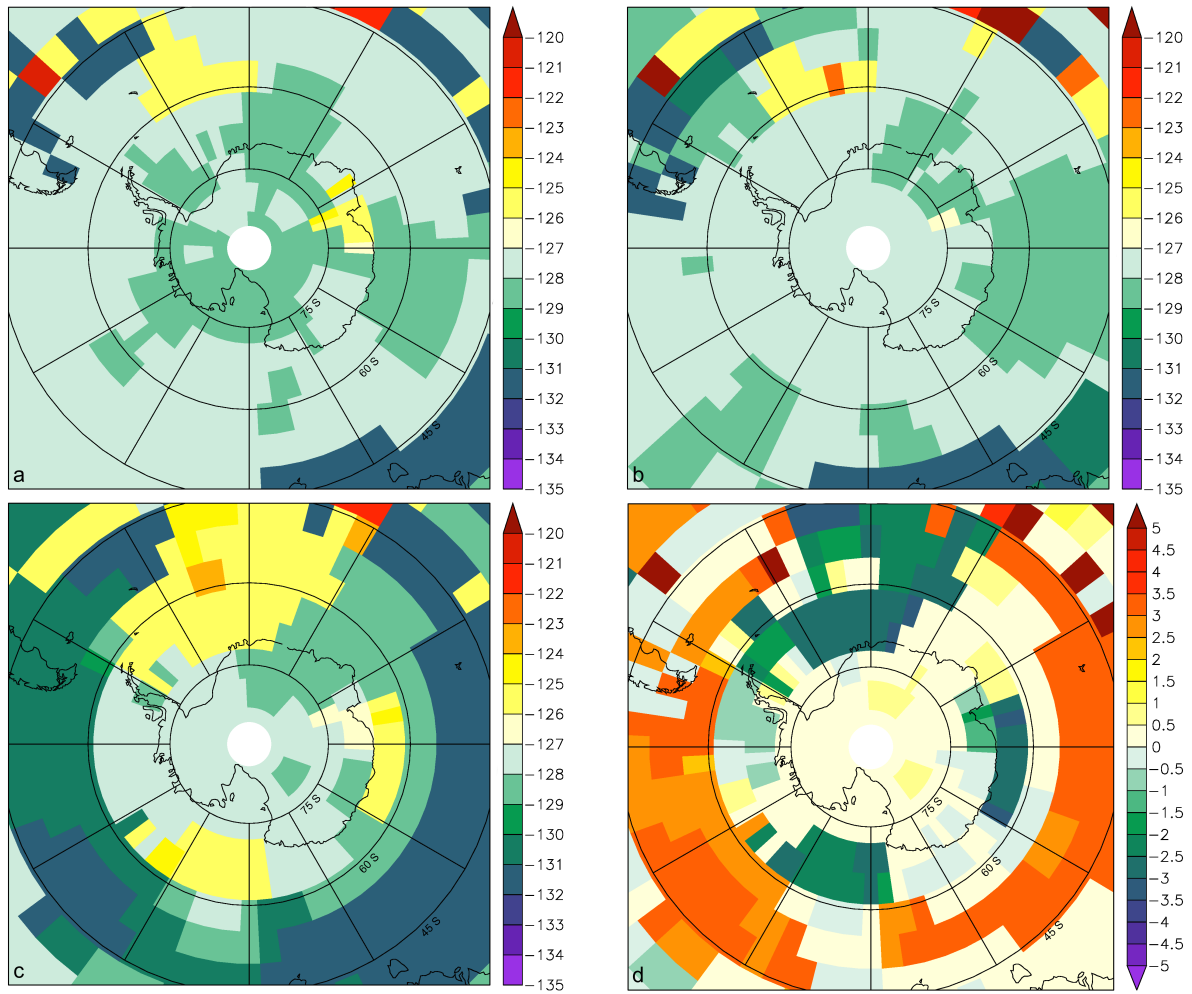
831 **Figure 7: Freshwater forcing and oceanic response characteristics. NH (a) and Antarctic ice sheet**  
 832 **freshwater fluxes (f), strength of the AMOC (b), NH sea ice area (c), SH sea ice area (d) and strength of**  
 833 **AABW formation (e) for the different experiments with and without freshwater forcing from Greenland,**  
 834 **Antarctic and NH ice sheet melting. Curves are smoothed with a running mean of 200 years for better**  
 835 **comparison.**  
 836



837 **Figure 8: Evolution of annual mean sea surface temperature (a) and mid-depth (485-700 m) ocean**  
 838 **temperature (b) anomalies relative to the pre-industrial in close proximity to the AIS (south of 63°S). (c)**  
 839 **Meltwater related changes in annual mean sea ice area at 129.5 kyr BP from differences between**  
 840 **experiments Reference and noAGfwf in per cent. The blue contour outlines the observed ice-shelf edge**  
 841 **and grounded ice margin of the present-day AIS for illustration. All curves (a, b) are smoothed with a**  
 842 **running mean of 200 years for better comparison.**

843

844



845

846 **Figure 9: Time of maximum surface air temperature (MWT) in kyr BP for experiments Reference (a),**

847 **noGfwf (b) and noAGfwf (c) and difference in MWT between experiments noGfwf and noAGfwf (d) in**

848 **kyr, showing the shift of the MWT when Antarctic freshwater fluxes are included.**

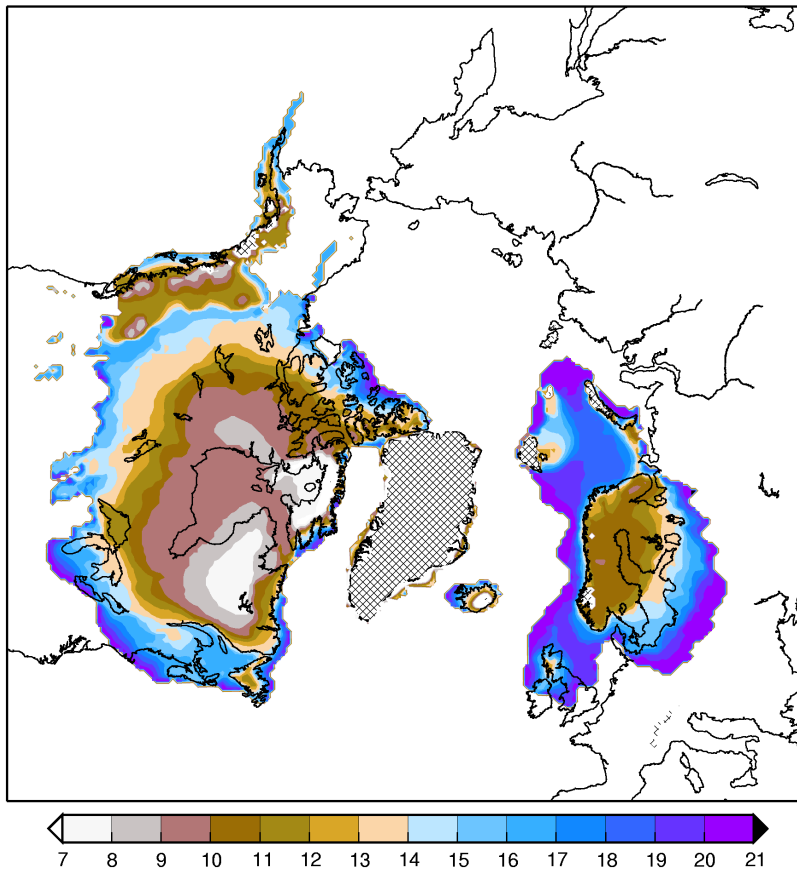
849

850

851 **Table A1: Sources of geomorphological data or modelling results used to prescribe changes in Northern**  
 852 **Hemisphere ice sheet extent for the retreat during Termination I.**

Ice Sheet	Source	Isochrone Time Period (kyr BP)
Laurentide	Dyke and Prest (1987)	18 – Present Day
Innuitian	Dyke et al. (2002)	18
Cordilleran	Clague and James (2002)	20 – Present Day (south)
	Dyke et al. (2002)	
	Mayewski et al. (1981)	18 (north) 21 – 7 (interior)
Iceland	Andersen (1981)	20 – Present Day
Eurasian	Andersen (1981)	20 – Present Day
	Landvik et al. (1998)	15 – 12 (Barents Sea)
	Mangerud et al. (2002)	18 (Southern Barents and Kara Seas)
	Svendsen et al. (1999)	18
European Alps	Zweck and Huybrechts (2003)	21 – Present Day (modelled ice extent)

853



854

855

856

**Figure A1: Interpolated ice sheet extent during the last deglaciation for the Northern Hemisphere ice sheets as a function of time (kyr BP). Hatched regions indicate present-day ice.**